A New Polymeric Minimally Invasive Glaucoma Implant

Document status and date:
Published: 06/05/2024

Document Version:
Publisher's PDF, also known as Version of Record (includes final page, issue and volume numbers)

Please check the document version of this publication:

• A submitted manuscript is the version of the article upon submission and before peer-review. There can be important differences between the submitted version and the official published version of record. People interested in the research are advised to contact the author for the final version of the publication, or visit the DOI to the publisher's website.
• The final author version and the galley proof are versions of the publication after peer review.
• The final published version features the final layout of the paper including the volume, issue and page numbers.

Link to publication

Download date: 19. Jun. 2025

A New Polymeric Minimally Invasive Glaucoma Implant

Inês C.F. Pereira, Paul A.A. Bartels, Christian J.F. Bertens, Serge H.M. Söntjens, Hans M. Wyss, Albertus P.H.J. Schenning, Patricia Y.W. Dankers, Henny J.M. Beckers, and Jaap M.J. den Toonder*

Glaucoma drainage devices are implanted in the eye to treat glaucoma, a disease that can cause vision loss and blindness. These devices are designed to reduce intraocular pressure (IOP), a major risk factor for the progression of glaucoma, by providing an alternative outflow path for the fluid produced by the eye, the aqueous humor. Here, a novel polymeric minimally invasive glaucoma implant designed to enhance aqueous humor outflow is demonstrated. The implant is made of a unique, potentially biodegradable thermoplastic material, polycarbonate bisamide (PC-BA), and produced through replica molding using hot embossing and femtosecond laser-machined glass molds. Post-mortem experiments demonstrate successful device implantation into a rabbit's eye, with the implant remaining securely in place. Although the mass loss and changes in molecular weight observed in the in vitro degradation experiments are not significant within the tested times and degradation conditions, the PC-BA is a slow-degradation polymer that may take a few years to fully degrade. Thus, the implant will also slowly degrade and be absorbed by the body over time, leaving behind a natural outflow pathway. This potentially biodegradable glaucoma implant may represent a promising new approach for restoring outflow in a more natural way.

1. Introduction

Glaucoma is a disease of the optic nerve and a leading worldwide cause of irreversible vision loss.[1] In 2020, over 70 million people suffered from glaucoma, and this number is expected to increase to more than 100 million people by 2040.[2] Elevated intraocular pressure (IOP) is the primary risk factor for the development and progression of glaucoma. The main determinant of IOP is the fine-tuned equilibrium between the production and drainage of aqueous humor (internal eye fluid), and its homeostasis is of vital importance to overall eye health and function. Aqueous humor is produced and secreted by the ciliary body and drains out of the eye mainly through the trabecular meshwork into Schlemm's canal (represented in **Figure 1**). As the aqueous humor inflow rate is relatively stable, IOP is mainly regulated by the resistance to aqueous humor outflow.[3] In glaucomatous eyes, there is an increased resistance to aqueous humor outflow, which leads to elevated IOP.[4] Currently, lowering IOP remains the only proven treatment for stopping glaucoma disease progression and related visual field loss.[5] Ophthalmologists use a variety of approaches to lower IOP, including pharmaceutical drugs/medication (usually eye drops), laser procedures, and incisional surgeries. Surgery with implantation of a glaucoma drainage device is often performed when the maximum tol-

I. C. Pereira, H. M. Wyss, J. M. den Toonder
Microsystems Research Section
Department of Mechanical Engineering
Eindhoven University of Technology
P.O. Box 513, Eindhoven 5600 MB, The Netherlands
E-mail: j.m.j.d.toonder@tue.nl

I. C. Pereira, P. A. Bartels, H. M. Wyss, A. P. Schenning, P. Y. Dankers,
J. M. den Toonder
Institute for Complex Molecular Systems (ICMS)
Eindhoven University of Technology
Den Dolech 2, Eindhoven 5600 MB, The Netherlands

P. A. Bartels, P. Y. Dankers
Laboratory of Chemical Biology
Department of Biomedical Engineering
Eindhoven University of Technology
P.O. Box 513, Eindhoven 5600 MB, The Netherlands

C. J. Bertens, H. J. Beckers
University Eye Clinic Maastricht
Maastricht University Medical Centre+ (MUMC+)
P. Debyelaan 25, Eindhoven 6229 HX, The Netherlands

S. H. Söntjens
SyMO-Chem BV
Den Dolech 2, Eindhoven 5612 AZ, The Netherlands

A. P. Schenning
Stimuli-Responsive Functional Materials & Devices
Department of Chemical Engineering and Chemistry
Eindhoven University of Technology
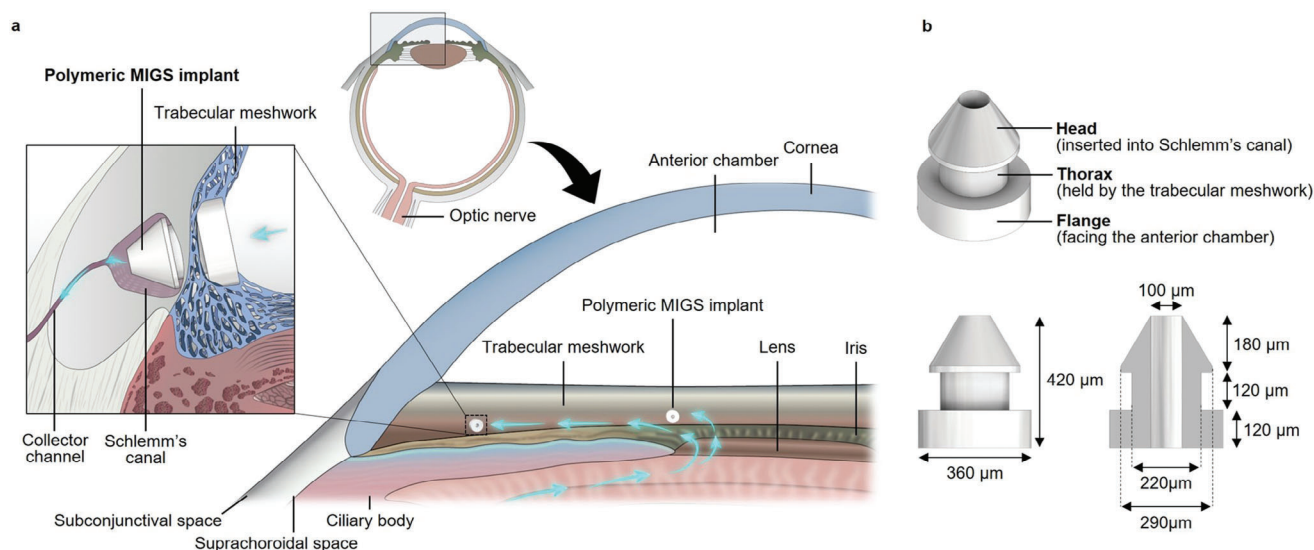Eindhoven 5600 MB, The Netherlands

Figure 1. Design and dimensions of the polymeric Schlemm's canal MIGS implant and its placement in the eye. a) Illustration showing the implant placement in the eye, with its flange facing the anterior chamber and its head inserted into Schlemm's canal; the blue arrows represent the direction of aqueous humor outflow from the anterior chamber, through the implant and into Schlemm's canal/collector channel. b) Schematic depiction of the implant design and its relevant dimensions.

erated medical/laser treatments fail to sufficiently lower IOP and prevent disease progression.[6] Glaucoma drainage devices can be categorized as either aqueous shunts with a tube-plate design or minimally invasive glaucoma surgery (MIGS) devices.[7–11] When compared to aqueous shunts, MIGS devices help to reduce the IOP with minimal tissue manipulation/destruction and are associated with a relatively good safety profile, short surgery time, and rapid recovery.[12] To date, the available MIGS offer a more modest IOP-lowering effect than aqueous shunts, but they have the benefit of a safer risk profile.[13,14]

Among the different MIGS devices available, the most popular ones are those that bypass the trabecular meshwork and directly shunt aqueous humor into Schlemm's canal, hence being referred to as Schlemm's canal MIGS devices.[15,16] Currently, the two most commonly used Schlemm's canal MIGS devices are the iStent *inject* (Glaukos Corporation, California, USA) and the Hydrus Microstent (Ivantis, Inc., California, USA).[17] The iStent *inject* is the world's smallest medical device known to be implanted in the human body.[18] It is made of heparin-coated implant-grade titanium and is inserted *ab interno* through a microincision made in the anterior chamber using an injection device (injector).[15] Overall, the iStent *inject* has been shown to be a safe and effective procedure in the treatment of different types of open-angle glaucoma in several clinical studies, either as a standalone procedure or combined with cataract surgery; the results showed most patients experienced a clinically significant lowering of IOP and a reduction in reliance on glaucoma medication, with a low incidence of postoperative complications.[15,18–26] The most common adverse events reported so far include stent malposition and obstruction, and transient hyphema (collection of blood inside the anterior chamber).[19–24,27–31]

Here, we propose a new polymeric Schlemm's canal MIGS implant with a design and dimensions similar to the newer ver-

sion of the iStent *inject*, the iStent *inject* W. The material we use to fabricate this device is a hydrogen-bonding polycarbonate bisamide (PC-BA) polymer. This thermoplastic PC-BA polymer was engineered both to meet the demands of hot embossing used for implant fabrication and to possess adequate mechanical properties necessary for the implants. The implants need to have sufficient stiffness to prevent permanent deformation when fabricated and handled during implantation. Also, the polymer should have some flexibility and softness to prevent complications such as endothelial cell loss, which can be caused by stiffer and harder metallic implants. A polymeric implant is also advantageous in avoiding problems with magnetic resonance imaging (MRI) associated with metallic implants. Moreover, many patients prefer not to have permanent metal implants in their eyes, and therefore, a polymeric implant could serve as a viable alternative.

The PC-BA polymer comprising our implant was additionally designed to be potentially biodegradable and to degrade slowly, primarily through the hydrolysis of the carbonate and amide groups.[32] The slow degradation of the PC-BA implant should offer enough time for a proper and sufficient remodeling of the trabecular meshwork to occur around the implant, and when degradation is completed, the extra outflow site created by the implant may remain patent, thus creating a long-term modification of the trabecular meshwork without the need for a permanent implant. The implant being biodegradable would be additionally advantageous in case it is mispositioned, becomes dislodged, or if the implant is overgrown by fibrotic material. As the device will degrade over time, there will be no accumulation of "lost" implants inside the eye. Thus, our implant is expected to offer similar positive outcomes as the iStent *inject* W due to the similar design, but with the additional benefit of being a non-metallic and, possibly, a non-permanent implant that will be naturally absorbed by the body over time.
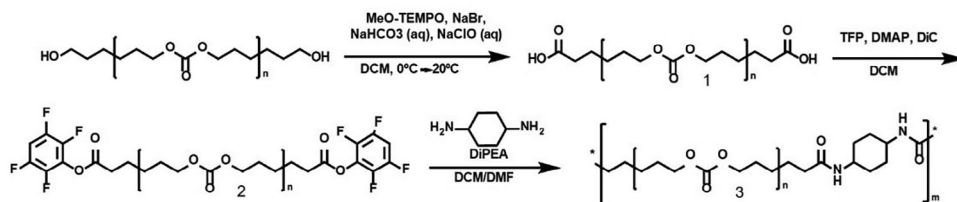
ADVANCED
SCIENCE NEWS

www.advancedsciencenews.com

ADVANCED
MATERIALS
TECHNOLOGIES

www.advmattechnol.de

Figure 2. Scheme of PC-BA synthesis starting with converting poly(hexamethylene carbonate) diol to a poly(hexamethylene carbonate) di-carboxylic acid (95% yield), and then reacting to a poly(hexamethylene carbonate) di-(tetra-fluorophenol active ester) (80% yield), which was reacted with trans-1,4-diaminocyclohexane to obtain the final polymer with a yield of 91%.

2. Implant Design

The design and dimensions of our new Schlemm's canal MIGS implant are shown in Figure 1b. It has radial symmetry, and is 420 µm-long and 360 µm-wide, resembling the iStent *inject* W. It is composed of three parts: a conical-shaped head designed to seat within Schlemm's canal; a wider flange, which faces the anterior chamber; and the thorax, which is retained by the trabecular meshwork, as illustrated in Figure 1a. The central lumen of the device through which the aqueous humor will flow has a diameter of 100 µm. With this device, a direct connection between the anterior chamber and the Schlemm's canal/collector channel is made, thus bypassing the trabecular meshwork. Apart from the material that our implant is made of, the main difference from the iStent *inject* W is that the latter contains four additional side outlets at the head of the stent, whereas our device only contains one central outlet. Also, the 100 µm lumen diameter of our device is larger than the 80 µm lumen diameter of the iStent *inject* W.

3. Results and Discussion

3.1. Synthesis and Characterization of Polycarbonate Bisamide

The thermoplastic PC-BA polymer used in this study was synthesized by reacting trans-1,4-diaminocyclohexane with the prepolymer poly(hexamethylene carbonate) di-(tetra-fluorophenol active ester), as schematically depicted in **Figure 2**. The activated prepolymer was synthesized by first converting a poly(hexamethylene carbonate) diol to a poly(hexamethylene carbonate) di-carboxylic acid with a yield of 95% and subsequently activating this telechelic di-acid with 2,3,5,6-tetrafluorophenol (80% yield). During the polymerization, the diamine ratio was slowly increased to one equivalent of the prepolymer, and the reaction was monitored with gel permeation chromatography (GPC). The polymer was obtained with a 91% yield. After purification, the polymer structure was confirmed with ^{1}H-NMR (Figure S1, Supporting Information).

The apparent number averaged molecular weight (M_n) of the hot embossed PC-BA polymer is 14.0 kg/mol and the weight averaged molecular weight (M_w) is 27.4 kg mol^{-1}, as determined from the GPC measurement (**Figure 3a**, Table S1, Supporting Information). A differential scanning calorimetry (DSC) measurement revealed that the polymer has a glass transition temperature for the PC soft block ≈−39.6 °C and three different melting transitions ≈8.2, 97, and 152.7 °C in the second heating run (Figure 3b; Table S1, Supporting Information). The melting transitions have enthalpies of 5.7, 0.09, and 2.9 J g^{-1}, respectively. The first melt-

ing peak originates from the soft polycarbonate block and the other two melting peaks originate from the melting of the amide hard block. The hard block has strong hydrogen bonding interactions resulting in a higher melting transition compared to the much weaker dipole interactions of the soft block. The molecular weights, glass transition temperature, and melting transitions of the polymer before hot embossing are similar to the values after the polymer has been hot embossed (Figure S2a,b,c, and Table S1, Supporting Information). Investigating the thermal stability of the polymer with thermogravimetric analysis reveals that the PC-BA starts to quickly degrade at a temperature ≈270 °C (Figure S2d, Supporting Information).

The mechanical behavior of the hot embossed material was determined with tensile testing and showed a typical stress-strain curve of a ductile thermoplastic (Figure 3c), undergoing yielding and extensive necking before it breaks. It can be seen from the graph that from 0 to ≈10 MPa, the PC-BA behaves as a linear elastic solid, with a Young's modulus of 45.8 ± 3.6 MPa. From 10 MPa plastic deformation begins, where the material stretches out considerably and a "neck" is formed. The neck extends and will continue to thin down until it breaks. As highlighted in the introduction, the PC-BA implant must possess adequate stiffness to resist permanent deformation during fabrication, and handling during implantation. The implants must be loaded into an injector delivery system before implantation into the trabecular meshwork, as explained later in this paper. Hence, the devices should be able to endure being grasped with tweezers during loading without deforming. Moreover, the injector delivery system exerts a significant amount of force when injecting the device into the trabecular meshwork. Thus, the implant should be tough enough to resist these forces and retain its original shape. However, the implant should also not be overly rigid, as this would make it very difficult to de-mold after the hot embossing process. The stress-strain curve demonstrates that the PC-BA polymer can withstand mechanical stress up to ≈10 MPa (60% strain) without undergoing permanent deformation. This implies that the stresses involved in the implant fabrication steps and subsequent handling likely remained below or around this limit, as no deformation was observed. Thus, we can conclude that the PC-BA polymer is an ideal polymer for the fabrication of the MIGS devices. The polymer can withstand the hot embossing process used for implant fabrication without significantly affecting its polymer structure and mechanical properties.

The cytotoxicity of the embossed PC-BA on primary human Tenon's capsule fibroblasts was investigated by means of a lactate dehydrogenase (LDH) release assay. LDH is released into the cell culture medium upon damage to the cell's plasma membrane.
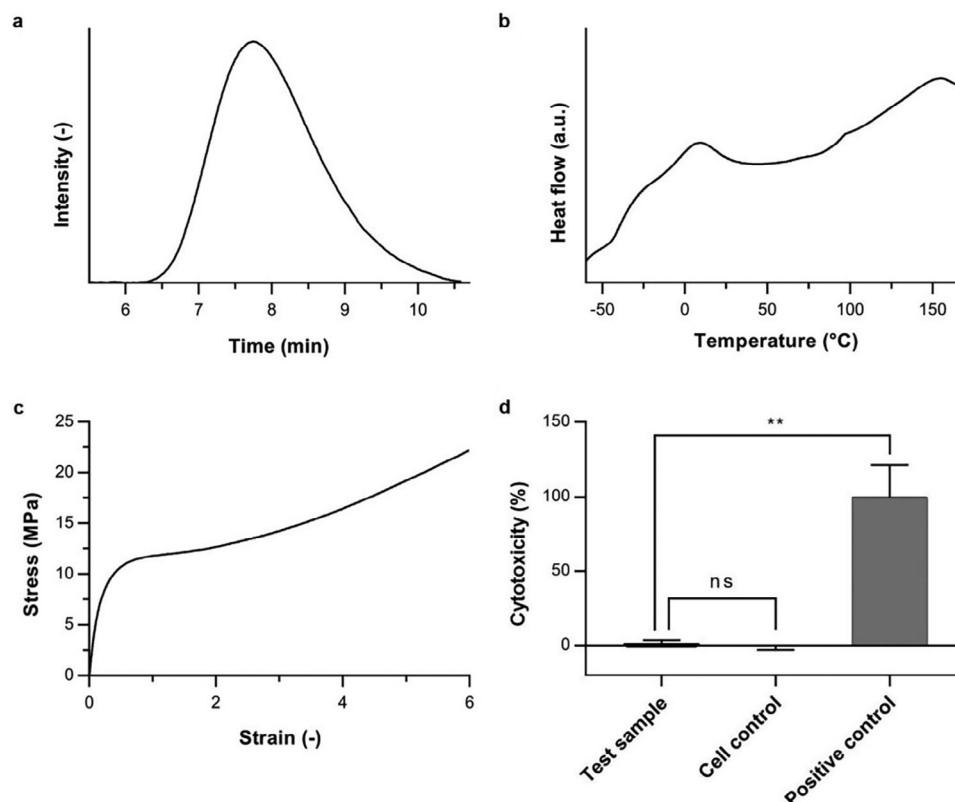
Figure 3. Characterization of the hot embossed PC-BA. a) Chromatogram measured with GPC, from which an apparent number averaged molecular weight $M_n = 14.0$ kg mol^{-1} and weight averaged molecular weight $M_w = 27.4$ kg mol^{-1} are determined. b) Second heating run of the hot embossed polymer measured with DSC. c) Stress-strain curve obtained from the average of three measurements in tensile testing ($n = 3$ samples tested), from which Young's modulus of 45.8 ± 3.6 MPa can be calculated. d) Calculated percentage of cytotoxicity of the PC-BA on primary human Tenon's capsule fibroblasts; each bar represents the mean $\pm$ SD ($n = 3$). ** represents $p \leq 0.01$ and "ns" represents a non-statistically significant difference as analyzed by two-way ANOVA with Tukey's multiple comparisons test.

The percentage of cytotoxicity obtained for all test conditions is shown in Figure 3d. The absorbance levels of formazan in the extracted culture medium used to calculate the cytotoxicity percentage are shown in Figure S3 (Supporting Information). This experiment reveals that the PC-BA polymer is non-cytotoxic.

3.2. Implant Fabrication and Characterization

We employed our own innovative microfabrication technique to fabricate the Schlemm's canal MIGS implant. The method involved replica molding using hot embossing and fused silica glass molds created by femtosecond laser micromachining, as demonstrated in **Figure 4b**. To the best of our knowledge, this is the first time that this method has been used to manufacture a biomedical implant. The molecular structure of the PC-BA polymer from which the implants are made is represented in Figure 4a, which also includes a schematic illustration of the stacking of the PC-BA polymer due to hydrogen bonds. As mentioned earlier, the mold used to give the PC-BA the shape indicated in Figure 1b was fabricated by femtosecond laser micromachining of fused silica glass. Femtosecond laser-assisted chemical wet etching is based on a two-step process of ultrashort-pulsed laser radiation in transparent materials, followed by chemical wet

etching to selectively remove the exposed material (Figure 4c).[33] The laser beam, focused inside the glass, locally modifies its refractive index and chemical properties, and patterns written by the laser are then chemically etched to form three-dimensional structures with high precision, aspect ratio, and complexity.[33,34] The complexity of the shape of our implant would be extremely difficult to achieve using classical micro-manufacturing techniques, such as photolithography or micro-milling.[35] A picture of the fabricated glass mold is shown in Figure 4d, which also includes a zoomed microscopic view of the features in the mold showing the 100 μm-diameter glass pillar used to form the central lumen of the implant. Using this mold, many implants can be fabricated in one single hot embossing step. In the hot embossing, we used 130 °C to melt the PC-BA polymer and five tons of pressure to help the melted polymer flow into the cavities of the mold (Figure 4b). The demolding took place after the hot embossing had cooled down to room temperature. Figure 4e shows a microscopic image of the fabricated implants. As can be seen, we were able to successfully transfer the features from the glass mold to the PC-BA polymer that comprises the implantable device using hot embossing. The glass mold was designed to produce implants with the dimensions shown in Figure 1b. After fabrication, the most relevant dimensions of our implants were measured, and the results are shown in Figure 4f. Our
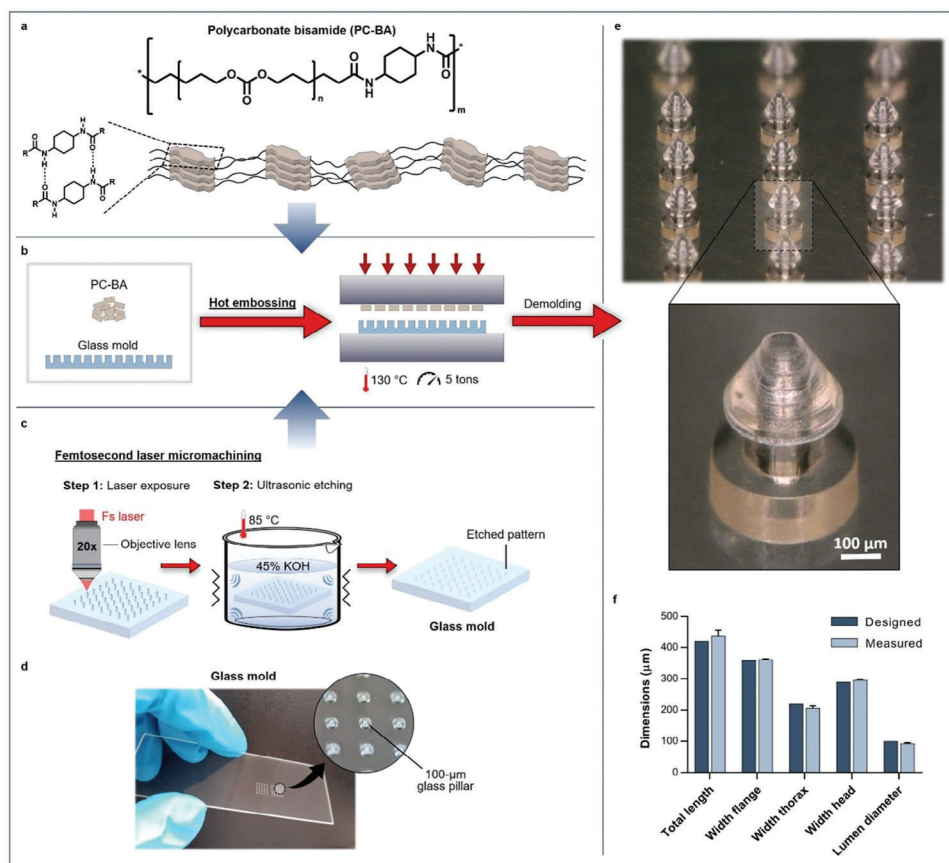
2301686 (4 of 10)

**ADVANCED
SCIENCE NEWS**

www.advancedsciencenews.com

**ADVANCED
MATERIALS
TECHNOLOGIES**

www.advmattechnol.de

Figure 4. The fabrication process of Schlemm's canal MIGS implant and its final shape and dimensions. a) Representation of the PC-BA molecular structure as well as a schematic illustration of the stacking of the PC-BA polymer due to hydrogen bonds. b) Schematic representation of the implant fabrication by replica molding using hot embossing, with femtosecond laser-machined fused silica glass molds. c) Schematic illustration of the femtosecond laser machining process used to fabricate the glass molds. d) Picture of the glass mold, made using femtosecond laser machining, used in the hot embossing of the implants. e) Demolded array of implants. f) Graph indicating the differences between the measured dimensions of the implant and the initially designed ones. The data represents the mean $\pm$ SD ($n = 5$).

implants have tolerances for the length of 438 $\pm$ 17.93 µm, the width of the flange of 362.20 $\pm$ 1.64 µm, the width of the thorax of 207 $\pm$ 6.44 µm, the width of the head of 296.60 $\pm$ 2.19 µm, and lumen diameter of 93 $\pm$ 2.92 µm. The length of the implants varied quite significantly, however, this was expected since the residual layer attached to the flange of the implants was manually removed with a razor blade after the demolding step, making it therefore very difficult to guarantee the same length across all the fabricated implants. Apart from the length, there are some minor deviations between the implant dimensions achieved after fabrication and those designed, as can be inferred from Figure 4f. These deviations can be explained by the size of the elliptical-shaped laser-affected zone during the femtosecond laser exposure, which, in fused silica glass and when using a 20x objective, is 3 µm-wide and 24 µm-long.[36] Nevertheless, these differences are not significant for the final application.

In this study, we have then demonstrated that the combination of hot embossing of thermoplastic materials with femtosecond laser-machined glass molds is a potentially advantageous process for mass production of micro-devices containing three-dimensional structures requiring a few micrometers resolution, high accuracy, and complexity.[37]

3.3. In Vitro Testing of the iStent *inject* W Injector

Since the dimensions and shape of our implant are very similar to the iStent *inject* W, we used the same injector delivery system to test the implantation of our device. The design and components that comprise the injector device are represented in **Figure 5**. The working principle of the injector is explained in the patent no. US010271989B2[38] and in the Supplementary Information.

With a small adaptation of the injector housing, detailed in the Supplementary Information and shown in Figure S4 (Supporting Information), we were able to repeatedly reload the injector device of the iStent *inject* W with our implants. The reloading with our implants was performed under microscopic view and with the help of sharp and thin-pointed tweezers, as demonstrated in Video S1, Supporting Information. In this video, we show that the recharged injector successfully injects our implant into a spongy-like substrate, a very simplified in vitro model of the trabecular meshwork porous structure. As can be seen in the video, the implant stays fixed and correctly positioned into the sponge, i.e., with the flange at the surface of the sponge and facing the camera used for recording.
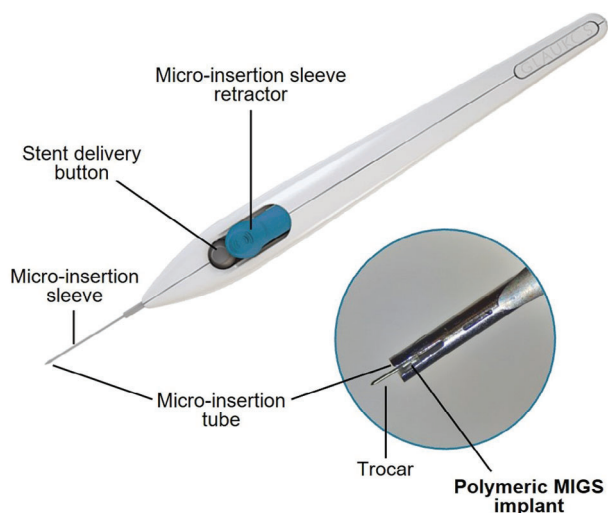
**ADVANCED
SCIENCE NEWS**

www.advancedsciencenews.com

**ADVANCED
MATERIALS
TECHNOLOGIES**

www.advmattechnol.de

Figure 5. Design and components that comprise the injector device of the iStent *inject* W; the zoomed figure shows the injector tip reloaded with one of our implants.

3.4. Post-Mortem Study

We performed a *post-mortem* experiment on the eye of a dead New Zealand White rabbit to investigate if the modified injector delivery system is capable of injecting our devices into a real trabecular meshwork as it does for the iStent *inject* W. For this experiment, the injector device was first reloaded with our implant as previously demonstrated in Video S1, Supporting Information. Subsequently, a corneal incision was made in the eye, and the injector was inserted through it into the anterior chamber to deliver our implant into the trabecular meshwork. A video of the implantation procedure was recorded (Video S2, Supporting Information), which confirms that our implant was successfully delivered into the trabecular meshwork. The zoomed picture shown in **Figure 6**, also included in Video S2, Supporting Information, shows that the flange of our device is visible in the anterior chamber, proving the proper placement of the implant in the trabecular meshwork.
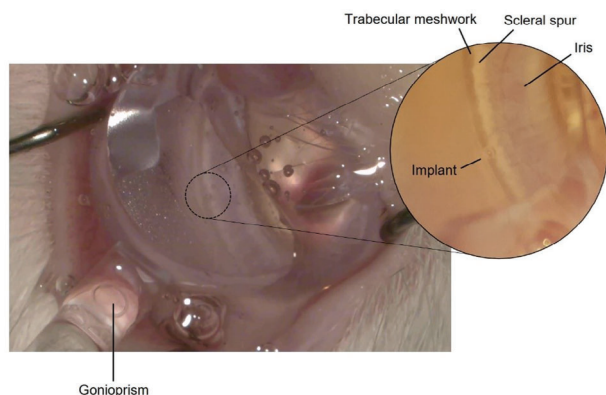

Figure 6. Picture showing the proper placement of our Schlemm's canal MIGS implant into the trabecular meshwork of the eye of a *post-mortem* rabbit, after being delivered by the modified injector device.

3.5. In Vitro Degradation

Degradation of the hot embossed PC-BA polymer via hydrolytic or oxidative pathways was studied. The hydrolytic pathway was investigated by incubating the polymeric material in phosphate-buffered saline (PBS, pH 7.4) in an accelerated experiment at 70 °C to study hydrolysis for 2, 30, and 60 days. After 60 days, a 1% mass loss was observed in the hydrolytic experiment in PBS, as shown in **Figure 7a**. The M_n of the polymer did not change after two days of incubation, but it decreased from 16.7 ± 0.8 kg mol^{-1} to 13.8 ± 0.7 kg mol^{-1} after 30 days, and after 60 days the molecular weight decreased further to 12.8 ± 0.6 kg mol^{-1} (Figure 7b, Table S2, Supporting Information). Enzyme-mediated hydrolysis was studied by incubating the material in lipase at 37 °C for 2, 7, and 14 days. After 14 days, a small decrease in mass of 1%–2% was observed (Figure 7a). The M_n was 13.2 ± 0.8 kg mol^{-1} after two days and it did not decrease further with 7 or 14 days of incubation (Figure 7b, Table S2, Supporting Information). Simulated oxidative degradation was investigated by incubating the polymeric material in a solution of 0.1 M Co(II)Cl$_2$·6H$_2$O in 20% (w/w) H$_2$O$_2$ in de-ionized (DI) water at 37 °C for 2, 7 and 14 days. No mass loss of the material was observed after 14 days (Figure 7a). The molecular weight of the polymer under oxidative degradation showed similar behavior to that under enzymatic degradation. The M_n was 13.5 ± 0.1 kg mol^{-1} after two days and it did not decrease any further (Figure 7b, Table S2, Supporting Information).

Overall, our in vitro degradation experiments did not show significant mass loss or changes in molecular weight within the tested times and degradation conditions. However, our results seem to suggest that the PC-BA polymer favors hydrolytic degradation over oxidative degradation. Thus, we expect the PC-BA to be a slow-degradation polymer that mainly degrades through hydrolysis of the carbonate and amide groups, either through interaction with water or enzymatic reactions.[32] It is known that carbonate and amide groups degrade slower than esters, which are very common in other biodegradable polymers such as polycaprolactone and polylactic acid.[39] We should note that the shape and morphology of the implants can also influence the degradation rate.[40] A nonporous dense material like that of the implants presented in this study degrades slower than a porous scaffold, for example. Moreover, in vivo conditions and implantation location also have an influence on the degradation behavior.[41,42] Hence, it is necessary to conduct additional long-term degradation studies in vitro, to determine whether the observed small changes in mass and molecular weight reported above are indeed indicative of polymer degradation. Additionally, in vivo studies in living glaucoma animal models are essential to validate our initial hypothesis that a biodegradable glaucoma drainage device could induce a long-term modification of the trabecular meshwork, resulting in a permanent extra outflow site after the implant's degradation is complete.

4. Conclusion

This study proposes a new polymeric, minimally invasive, and potentially biodegradable, glaucoma drainage device that is designed to be inserted into Schlemm's canal to enhance the outflow of aqueous humor from the anterior chamber, thereby
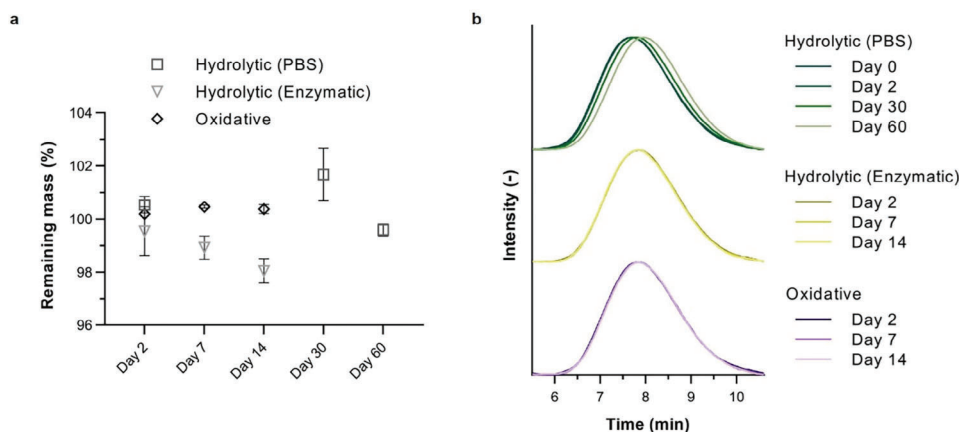
**ADVANCED
SCIENCE NEWS**

www.advancedsciencenews.com

**ADVANCED
MATERIALS
TECHNOLOGIES**

www.advmattechnol.de

Figure 7. PC-BA characterization after degradation through exposure to hydrolytic or oxidative environments. a) Mass loss measured after 2, 30, and 60 days for the samples exposed to a hydrolytic environment through incubation with a PBS solution (pH 7.4) at 70 °C and after 2, 7, and 14 days for the samples in enzymatic solution at 37 °C, and in an oxidative environment after 2, 7 and 14 days at 37 °C. b) Chromatogram measured with GPC of the polymer before and after 2, 30, and 60 days for samples in hydrolytic PBS solution at 70 °C, and after 2, 7, and 14 days for samples in enzymatic and oxidative environments at 37 °C.

reducing IOP. The design of our device was inspired by the currently available iStent *inject* W, the world's smallest medical device known to be implanted in the human body that has been proven to be generally safe and effective in treating glaucoma. Unlike the iStent *inject* W, which is made of heparin-coated titanium, our device is made of a polymeric material called polycarbonate bisamide, or PC-BA. We have demonstrated that this material is biocompatible and possesses ideal mechanical properties – it can withstand the hot embossing process used for implant fabrication and handling during implantation without undergoing permanent deformation. Additionally, we anticipate that PC-BA is a slow-degrading polymer, which might take a few years to be fully reabsorbed by the body. This slow degradation may provide enough time for proper and sufficient remodeling of the trabecular meshwork to occur around the implant, and, when degradation is completed, this might leave a patent outflow site without the need for a permanent implant that could potentially scar over time and lose effectiveness.

Since our implant has a shape and dimensions comparable with the iStent *inject* W, we used the same injector delivery system to test the implantation of our device. With a small adaptation of the injector housing, we were able to repeatedly reload the injector with our implants. Our first in vitro implantation test demonstrated that the recharged injector successfully injected the implant into a spongy-like substrate, a very simplified in vitro model of the trabecular meshwork porous structure. The implant stays fixed and correctly positioned within the sponge. Furthermore, a *post-mortem* experiment performed on a rabbit eye confirmed that the modified injector device is capable of correctly injecting our implants into a real trabecular meshwork as it does for the iStent *inject* W.

The presented work introduces the concept and shows the proof-of-principle of our polymeric, and potentially biodegradable, glaucoma implant. However, further research and development are needed for application in clinical practice. In future work, we will investigate the biocompatibility, biodegradability, and effectiveness of our device in reducing IOP by conducting in

vivo experiments using an animal model. Given that the degradation rate of the device can be affected by the specific in vivo environment, it is essential to perform such long-term animal experiments to gain a better understanding and quantification of its degradation behavior and to investigate how the trabecular meshwork tissue adapts and, as we anticipate, grows around the implant over time. Additionally, these studies will help us verify our initial hypothesis that our new implant can create a long-term modification of the trabecular meshwork and leave a permanent extra outflow site that will not be scarred or closed after the device has been fully absorbed into the body.

5. Experimental Section

Synthesis and Characterization of Polycarbonate Bisamide: All reagents, chemicals, materials, and solvents were obtained from commercial sources and used without further purification, except the poly(hexamethylene carbonate) diol, which was generously provided by Bayer. Drying of solvents, when necessary, was done using molsieves. Reactions were run under an inert atmosphere (Ar) whenever appropriate. ^{1}H-NMR spectroscopy was performed using either a Varian Mercury or a Bruker AVANCE III HD spectrometer at 400 MHz and 298 K. All shifts were reported with respect to TMS at 0 ppm. Infrared spectroscopy was performed using a Perkin Elmer Spectrum One ATR FT-IR spectrometer. Gel permeation chromatography (GPC, SEC) was performed on Varian/Polymer Laboratories PL-GPC 50 equipment using a Shodex GPC KD-804 column that was operated at 50 °C using dimethylformamide, or DMF (with 10 mM LiBr and 0.3% water), as the eluent or on a Shimadzu LC-10ADVP system with a Shimadzu RID-10A refractive index detector, a Shimadzu SPD-M10AVP UV–Vis detector, and a combination of a PLgel 5-µm mixed-C column and a PLgel 5-µm mixed-D column, using tetrahydrofuran, or THF, as eluent.

Poly(Hexamethylene Carbonate) Di-Carboxylic Acid: Telechelic poly(hexamethylene carbonate) diol (M_n = 2.0 kg mol^{-1}; 32 g, 16 mmol) was dissolved in 150 mL dichloromethane. MeO-TEMPO (0.1 g, 0.5 mmol) was added to this DCM solution, as well as a solution of NaBr (0.7 g, 7 mmol) in 200 mL 1 M NaHCO$_3$. The resulting two-phase system was stirred vigorously and cooled in an ice bath. Aqueous NaOCl (13%, ≈3.7 M, 60 mL) was added slowly to the reaction mixture, which

**ADVANCED
SCIENCE NEWS**

www.advancedsciencenews.com

**ADVANCED
MATERIALS
TECHNOLOGIES**

www.advmattechnol.de

was allowed to warm to room temperature after the addition of the hypochlorite. Stirring was continued for 1 h, after which ^{1}H NMR confirmed full conversion of the alcohol end groups. The reaction mixture was subsequently cooled in an ice bath and adjusted to pH 1–2 with a concentrated aqueous HCl solution. The organic phase was separated from the aqueous phase, which was subsequently extracted with CHCl$_3$ (2 × 100 mL). The combined organic phases were washed with water (150 mL), dried with MgSO$_4$, and evaporated to yield the crude product (colorless oil). This oil was stirred vigorously with di-isopropyl ether (iPr$_2$O; 100 mL), after which the product was allowed to settle at −20 °C overnight. The supernatant was removed, and the resulting white solid was dried *in vacuo* to yield 30.8 g (95%) of the desired material 1.

^{1}H-NMR (400 MHz, CDCl$_3$): δ = 4.1 (t, n*4H), 2.4 (t, 4H, CH$_2$COOH), 1.8–1.2 (br. m, CH$_2$) ppm. No CH$_2$OH protons were detectable by NMR, confirming full conversion. FT-IR (ATR): ν = 2940, 2885, 1740, 1588, 1465, 1404, 1251, 1067, 957, 792, 735 cm^{-1}. ^{1}H NMR showed n≈15.5 (M$_n$ = ca. 2.4 kg mol^{-1}). GPC (THF): M$_n$ = 4.7 kg mol^{-1}; PDI = 1.75.

Poly(Hexamethylene Carbonate) Di-(Tetra-Fluorophenol Active Ester): Telechelic poly(hexamethylene carbonate) di-carboxylic acid 1 (20 g, 8.7 mmol) was dissolved in DCM (75 mL) with 2,3,5,6-tetrafluorophenol (3.6 g, 22 mmol) and DMAP (89 mg). N,N'-diisopropylcarbodiimide (DiC, 3.6 mL, 23 mmol) was added to the reaction mixture, causing almost immediate formation of a crystalline precipitate. After 3 h, NMR confirmed the full conversion of the two carboxylic acid end groups to active ester end groups. The reaction mixture was filtered, evaporated to dryness, stirred with n-pentane, and decanted (2x) to afford the crude product as a white solid. This solid was redissolved in toluene, stirred with flash silica to remove impurities, filtered, and evaporated to dryness. The resulting solid was again dissolved in toluene, stirred with a mixture of flash silica and MgSO$_4$, filtered, and evaporated to dryness. This procedure was repeated twice more with just flash silica and using chloroform as the solvent. The resulting solid was stirred with n-pentane, allowed to settle at −20 °C, decanted, and dried in vacuo to yield 18.2 g (80%) of the prepolymer product two.

^{1}H-NMR (400 MHz, CDCl$_3$): δ = 7.0 (q, 2H), 4.1 (t, n*4H), 2.7 (t, 4H, CH$_2$COO), 1.8–1.2 (br. m, CH$_2$) ppm. FT-IR (ATR): ν = 2940, 2870, 1789, 1733, 1645, 1525, 1485, 1466, 1406, 1346, 1329, 1240, 1180, 1083, 1070, 935, 791, 735, 716 cm^{-1}. ^{1}H-NMR showed n ≈16.1 (M$_n$ = ca. 2.8 kg mol^{-1}).

Poly(Hexamethylene Carbonate) 1,4-Cyclohexyl Bisamide, P6C-A[6]A: Prepolymer 2 (18 g, 6.3 mmol), DIPEA (5.6 mL, 32 mmol), and trans-1,4-diaminocyclohexane (0.686 g, 6.0 mmol, 0.95 eq.) were dissolved in a mixture of 50 mL DCM and 20 mL DMF. The reaction mixture was initially turbid but became clear and more viscous over time. After stirring for 16 h an aliquot was analyzed with NMR and GPC. To improve the chain extension another 0.2 g of the prepolymer two and, in steps over the next 40 h while checking with GPC, 25.4, 11.8, and 8.3 mg of the diamine were added, gradually increasing the diamine ratio to 1.0 equivalents with respect to two. The resulting material was precipitated in a mixture of 1.2 L MeOH and 0.2 L water, decanted, stirred with 0.5 L MeOH, decanted, and dried in vacuo at 50 °C. The resulting material was redissolved in 100 mL CHCl$_3$ with 30 mL MeOH and reprecipitated in 1 L MeOH, decanted, and dried in vacuo at 60°C, yielding 15.3 g of a tan, rubbery solid (91%).

^{1}H-NMR (400 MHz, CDCl$_3$): δ = 5.3 (br. s, 2H), 4.1 (t, n*4H), 3.8 (br. s, 2H), 2.1 (t, 4H), 2.0 (m, 4H), 1.8–1.3 (br. m, CH$_2$), 1.2 (m, 4H) ppm. FT-IR (ATR): ν = 3294, 2938, 2861, 1737, 1637, 1544, 1464, 1403, 1240, 1062, 960, 904, 792, 731 cm^{-1}.

Differential Scanning Calorimetry: The material was weighed and sealed in Tzero aluminum pans before DSC measurements were done on a DSC Q2000 (TA instruments, United States). The samples were first brought to an isotropic state at 40 °C and then heated to 180 °C at 10 °C min^{-1}, which marked the first heating run and cooled to −70 °C at the same rate. Then the material was further subjected to two heating/cooling cycles from −70 to 180 °C with a heating/cooling rate of 10 °C min^{-1}. The data was quantified and analyzed using Universal Analysis software (V4.5A, TA Instruments).

Mechanical Testing: A mechanical tensile test was performed on PC-BA thin films using a tensile test machine (ZwickRoell Z010) with a crosshead speed of 20 mm min^{-1} and a 100 N static load cell. For the preparation of the test specimens, first, a 200 µm-thick film was fabricated in a hot embossing machine (Specac Limited). 130 °C to melt the polymer and five tons of pressure to press the polymer into the shape of a film were used . The demolding took place after the hot embossing had cooled down to room temperature. Thereafter, the film obtained was cut into three small rectangular specimens of ≈30 × 10 × 0.2 mm (length × width x thickness). Young's modulus was determined as the slope of the linear portion of the obtained stress-strain curve.

Thermogravimetric Analysis: Measurements were done on a Perkin-Elmer TGA 7 using the high-resolution dynamic mode. Samples were put in platinum pans. The measurements were started at room temperature and heated to 400 °C at a heating rate of 10 °C min^{-1}, performed under an atmosphere of air or nitrogen (flow rate 20 mL mi^{-1}n).

In Vitro Cytotoxicity: To determine the cytotoxicity of the PC-BA polymer on primary human Tenon's capsule fibroblasts, the CyQUANT LDH cytotoxicity assay (Invitrogen, ThermoFisher Scientific) were used.[43,44] LDH release into the culture medium due to membrane damage of cultured cells was used as an indicator of cytotoxicity. For making the test samples used in this experiment, a 200 µm-thick film was first fabricated using hot embossing, and thereafter cut to small circular pieces of 7 mm in diameter. These served as representative samples of the final implant, processed in the same manner and using the same materials as the final implant, adhering to ISO 10993-12 (Biological evaluation of medical devices – Part 12: Sample preparation and reference materials). The samples were then sterilized by immersing in 70% ethanol for 20 min and treated with UV for 15 min, after which they were rinsed in PBS (pH 7.4) before transferring to a sterile 96-well plate. The cells were then seeded at 3.2 × 10^3 cells well^{-1} into the well plate containing the test samples (three replicates) using complete Advanced Dulbecco's modified Eagle Medium (DMEM) supplemented with 10% of Fetal Bovine Serum (FBS), 100 U mL^{-1} penicillin and streptomycin, and 0.2 mM L-glutamine (now referred to as culture medium). Cells were seeded in triplicate, after which they were incubated at 37 °C in 5% CO$_2$ for 48 h along with the positive and negative controls. Untreated cells in the culture medium alone served as negative control and were used to give the Spontaneous LDH activity. An amount of 10 µL of 10X Lysis Buffer was added to untreated cells (no contact with the test material) and used as the Maximum LDH Activity (positive control). After 45 min of incubation, 50 µL of the medium from all three conditions was collected and gently mixed with 50 µL of the Reaction Mixture in a new 96-well plate, and thereafter placed on ice for another 45 min. The absorbance of each well was then measured at 490 and 680 nm. To determine LDH activity, first, the absorbance at 680 nm (background signal from the instrument) was subtracted from the absorbance at 490 nm. The percentage of cytotoxicity was then calculated as follows

$$\% \ Cytotoxicity = 100 \times \frac{Treatment \ group \ activity \ - \ Negative \ control \ activity}{Positive \ control \ activity \ - \ Negative \ control \ activity} \quad (1)$$

In Vitro Degradation Experiment: The PC-BA polymer was subjected to accelerated hydrolytic degradation by exposition to PBS solution (pH 7.4) at 70 °C according to the international ISO 10993-13-2010 standard. The test samples used in this experiment were prepared as described above for the cytotoxicity experiment. Shortly, first a 200 µm-thick film was fabricated using hot embossing and thereafter cut into small circular pieces of 7 mm in diameter. The samples were thoroughly rinsed with 70% ethanol followed by DI water to remove any debris, after which they were individually inserted into 2 mL Eppendorf tubes and placed in a vacuum oven at 50 °C for 2 h for drying the samples to constant mass. Thereafter, the initial mass of the specimens was measured. PBS was then added to each Eppendorf tube and the samples were inserted into a water bath pre-heated to 70 °C. The sample to PBS ratio was ≈1 g:40 mL and sampling timepoints were 2, 30, and 60 days. At each time interval, the samples were removed from the PBS, washed with DI water, and subsequently dried to constant mass in a vacuum oven as previously described. Finally, the mass of the

**ADVANCED
SCIENCE NEWS**

www.advancedsciencenews.com

**ADVANCED
MATERIALS
TECHNOLOGIES**

www.advmattechnol.de

specimens after degradation was measured. The percentage mass change was determined using the following equation:

$$\% \ Remaining \ mass = 100 \times \frac{m}{m_i} \qquad (2)$$

where m is the mass of the degraded sample measured at each time point of the experiment and m_i is the initial mass of the test sample. After measuring the weight loss, the samples were used for GPC measurements by cutting a piece of the samples with the appropriate weight (3 mg mL^{-1} in DMF).

For the enzymatic and oxidative degradation experiments, a similar protocol was followed. However, instead of PBS, a solution of 500 U/mL lipase in PBS was used at 37 °C for the enzymatic degradation experiment, and a solution of 0.1 M Co(II)Cl$_2$·6H$_2$O in 20% (w/w) H$_2$O$_2$ in DI water was used at 37 °C for the oxidative degradation experiment, respectively. Additionally, the sampling time for this experiment was 2, 7, and 14 days, following published protocols.[45–47] Every 3–4 days the solution was refreshed. The washing of the samples was performed as mentioned above, but they were additionally centrifuged twice in DI water at 4000 rpm for 5 min.

Implant Fabrication and Characterization: The PC-BA MIGS implants were fabricated by replica molding using a hot embossing machine. The mold used in the hot embossing to give the PC-BA the desired shape of the implant was fabricated using a femtosecond laser machining process (Figure 4c). The design of the mold was prepared using the dedicated Alphacam software, where the laser scanning path (tool-path) to be fed to the FEMTOprinter f200 aHead (FEMTOprint SA, Switzerland) for exposing the fused silica glass, was also generated. The mold was fabricated on a 75 × 25 × 1 mm fused silica glass slide. The pulse energy and repetition rate used were 230 nJ and 1000 kHz, respectively. The laser was focused with a Thorlabs 20x microscope objective with a numerical aperture (NA) of 0.4. When the machining program was finished, the glass slide was immersed in a concentrated solution of 45% potassium hydroxide (KOH, Sigma-Aldrich) diluted in water to remove the exposed material. Finally, the mold was rinsed thoroughly with acetone and DI water to remove all debris. To facilitate the release (demolding) of the implants after the hot embossing step, the femtosecond laser-machined glass mold was first coated with a superhydrophobic layer of fluorosilane (Trichloro(1H,1H,2H,2H-perfluorooctyl)silane, Sigma-Aldrich). To improve the adhesion of this coating, the mold underwent an oxygen plasma treatment performed immediately before the fluorosilane vapor deposition. After the silanization treatment, the mold was ready to be used in the hot embossing machine together with the PC-BA pellets to fabricate the implants. 130 °C to melt the polymer and five tons of pressure to help the melted polymer flow into the cavities of the mold is used (Figure 4b). The demolding took place after the hot embossing had cooled down to room temperature. Afterward, the residual layer attached to the flange of the implants was removed by cutting it by hand using a razor blade under microscopic view.

The shape morphology, and key dimensions of the implant were observed and measured using a Keyence VHX-5000 digital microscope.

Injector: Injectors previously used in iStent *inject* W surgeries were provided by the University Eye Clinic, and Maastricht University Medical Center+. After creating the small window in the housing of the injectors using a soldering iron and a scalpel, they were recharged with the implants under microscopic view. To investigate if the injectors successfully deliver the MIGS implants, as they do for the iStent inject W, the injection process using a spongy-like substrate, a very simplified in vitro model of the trabecular meshwork porous structure were tested . A video showing the reloading of the injector with the implant and its delivery by the injector into the sponge was recorded (see Video S1, Supporting Information).

Post-Mortem Study: A *post-mortem* experiment was conducted on the eye of a fresh adult New Zealand White rabbit cadaver kindly provided by the Central Laboratory Facility of Maastricht University. This experiment aimed at investigating whether the devices were successfully delivered into a real trabecular meshwork using the modified injector device. For the im-

plantation procedure, first, a clear corneal incision was made with a 1 mm side port knife (KAI MEDICAL, Japan). Hereafter, a viscoelastic solution (Visco-elastic – Hyaluron, Medical Workshop, The Netherlands) was injected to deepen the anterior chamber and for better angle visualization. A gonioscopy was performed to ensure the presence of an open and clear angle suitable for the implantation of the device. Thereafter, the recharged injector was inserted through the corneal incision and the implant was delivered into the trabecular meshwork. Upon visual confirmation of the device's position in the trabecular meshwork, the delivery system was withdrawn. A video of the implantation procedure was recorded (see Video S2, Supporting Information).

Supporting Information

Supporting Information is available from the Wiley Online Library or from the author.

Conflict of Interest

The authors declare no conflict of interest.

Data Availability Statement

The data that support the findings of this study are available from the corresponding author upon reasonable request.

[1] K. S. Parikh, A. Josyula, R. Omiadze, J. Y. Ahn, Y. Ha, L. M. Ensign, J. Hanes, I. Pitha, *Sci. Rep.* **2020**, *10*, 12911.

[2] Y. C. Tham, X. Li, T. Y. Wong, H. A. Quigley, T. Aung, C. Y. Cheng, *Ophthalmology* **2014**, *121*, 2081.

[3] T. S. Acott, M. J. Kelley, K. E. Keller, J. A. Vranka, D. W. Abu-Hassan, X. Li, M. Aga, J. M. Bradley, *J. Ocul. Pharmacol. Ther.* **2014**, *30*, 94.

[4] N. H. Andrew, S. Akkach, R. J. Casson, *Surv Ophthalmol* **2020**, *65*, 18.

[5] J. Konopińska, K. Lewczuk, J. Jabłońska, Z. Mariak, M. Rękas, *Clinical Ophthalmology* **2021**, *15*, 1109.

[6] N. M. Kerr, J. Wang, K. Barton, *Clin. Exp. Ophthalmol.* **2017**, *45*, 393.

[7] S. J. Gedde, J. C. Schiffman, W. J. Feuer, L. W. Herndon, J. D. Brandt, D. L. Budenz, *Am. J. Ophthalmol.* **2012**, *153*, 789.

[8] P. G. Christakis, J. W. Kalenak, J. C. Tsai, D. Zurakowski, J. A. Kammer, P. J. Harasymowycz, J. J. Mura, L. B. Cantor, I. I. K. Ahmed, *Ophthalmology* **2016**, *123*, 2093.

[9] D. L. Budenz, K. Barton, S. J. Gedde, W. J. Feuer, J. Schiffman, V. P. Costa, D. G. Godfrey, Y. M. Buys, *Ophthalmology* **2015**, *122*, 308.

[10] P. G. Christakis, D. Zhang, D. L. Budenz, K. Barton, J. C. Tsai, I. I. K. Ahmed, *Am. J. Ophthalmol.* **2017**, *176*, 118.

[11] P. Bloom, L. Au, *Ophthalmol Ther* **2018**, *7*, 203.

[12] L. Bar-David, E. Z. Blumenthal, *Rambam Maimonides Med J* **2018**, *9*, e0024.

[13] G. M. Richter, A. L. Coleman, *Clinical Ophthalmology* **2016**, *10*, 189.

[14] E. Ansari, *Ophthalmol Ther* **2017**, *6*, 233.

[15] L. E. Pillunat, C. Erb, A. G. M. Jünemann, F. Kimmich, *Clinic. Ophthalmol.* **2017**, *11*, 1583.

[16] W. M. GRANT, *Arch. Ophthalmol.* **1963**, *69*, 783.

[17] I. C. F. Pereira, R. van de Wijdeven, H. M. Wyss, H. J. M. Beckers, J. M. J. den Toonder, *Eye* **2021**, *35*, 3202.

[18] C. C. A. Sng, K. Barton, Eds., *Minimally Invasive Glaucoma Surgery*, Springer, Singapore, **2017**.

[19] W. S. Shalaby, J. Jia, L. J. Katz, D. Lee, *J Cataract Refract Surg* **2021**, *47*, 385.

[20] F. H. Hengerer, G. U. Auffarth, I. Conrad-Hengerer, *Adv. Ther.* **2022**, *39*, 1417.

[21] T. W. Samuelson, S. R. Sarkisian, D. M. Lubeck, M. C. Stiles, Y. J. Duh, E. A. Romo, J. E. Giamporcaro, D. M. Hornbeak, L. J. Katz, W. Bartlett, C. Buznego, S. Johnson, F. A. D'Ambrosio, D. Dehning, H. DuBiner, R. Goyal, B. Hughes, R. E. Marquis, R. Noecker, S. Tauber, B. R. Perez, L. Roel, S. Sarkisian, S. Silverstein, S. Day, K. Solomon, F. Tyson, S. Vold, T. Samuelson, S. Simmons, et al., *Ophthalmology* **2019**, *126*, 811.

[22] Y. Y. Chen, Y. Y. Chen, Y. Y. Chen, Y. Y. Chen, Y. J. Lai, Y. J. Lai, Y. J. Lai, Y. F. Yen, Y. F. Yen, Y. F. Yen, L. Y. Huang, L. Y. Huang, L. Y. Huang, *J. Ophthalmol.* **2020**, *2020*, 8754730.

[23] P. R. Healey, C. I. Clement, N. M. Kerr, D. Tilden, L. Aghajanian, *J. Glaucoma.* **2021**, *30*, 606.

[24] P. Arriola-Villalobos, J. M. Martinez-De-La-Casa, D. Diaz-Valle, L. Morales-Fernandez, C. Fernandez-Perez, J. Garcia-Feijoo, *J. Ophthalmol.* **2016**, *2016*, 1056573.

[25] M. Fingeret, J. E. Dickerson, *Optomet. Vision Sci.* **2018**, *95*, 155.

[26] J. Konopińska, E. Saeed, Ł. Lisowski, K. Gołaszewska, P. Kraśnicki, D. A. Dmuchowska, I. Obuchowska, *J. Clin. Med* **2021**, *10*, 4410.

[27] B. C. H. Ang, W. Chiew, V. C. H. Yip, C. H. Chua, W. S. Han, I. O. C. Tecson, J. J. Ogle, B. A. Lim, O. K. Hee, E. L. Y. Tay, V. K. Y. Yong, H. T. Wong, L. W. L. Yip, *Eye Vision* **2022**, *9*, 27.

[28] C. E. C. Young, D. A. Ammar, L. K. Seibold, M. B. Pantcheva, J. R. SooHoo, M. Y. Kahook, *J. Glaucoma.* **2018**, *27*, 606.

[29] M. Shah, X. Campos-Möller, L. Werner, N. Mamalis, I. I. K. Ahmed, *J. Cataract Refract. Surg.* **2018**, *44*, 654.

[30] M. Shah, *Eye Vision* **2019**, *6*, 29.

[31] E. M. Schehlein, M. A. Kaleem, R. Swamy, O. J. Saeedi, *Expert Rev. Ophthalmol.* **2017**, *12*, 331.

[32] S. L. Bourke, J. Kohn, *Adv. Drug Deliv. Rev.* **2003**, *55*, 447.

[33] T. Suthisomboon, S. Bargiel, K. Rabenorosoa, E. Pengwang, in *2020 Symposium on Design, Test, Integration and Packaging of MEMS and MOEMS (DTIP)*, Lyon, France, **2020**, pp. 1–5.

[34] A. Steimle, *Laser Technik Journal* **2018**, *15*, 32.

[35] B. Bin Xu, Y. L. Zhang, H. Xia, W. F. Dong, H. Ding, H. B. Sun, *Lab Chip* **2013**, *13*, 1677.

[36] S. Rajesh, Y. Bellouard, *Opt. Express* **2010**, *18*, 21490.

[37] H. W. Choi, S. Bong, D. F. Farson, C. Lu, L. J. Lee, *J. Laser Appl.* **2009**, *21*, 196.

[38] D. S. Haffner, H. K. Gille, C. R. Kalina Jr., J. J. Cogger, System and Method for Delivering Multiple Ocular Implants, **2019**.

[39] M. Prakasam, J. Locs, K. Salma-Ancane, D. Loca, A. Largeteau, L. Berzina-Cimdina, *J. Funct. Biomater.* **2017**, *8*, 44.

[40] Y. Dong, S. Liao, M. Ngiam, C. K. Chan, S. Ramakrishna, *Tissue Eng. Part B Rev.* **2009**, *15*, 333.

[41] M. Bartnikowski, T. R. Dargaville, S. Ivanovski, D. W. Hutmacher, *Prog. Polym. Sci.* **2019**, *96*, 1.

[42] J. C. Tille, S. de Valence, D. Mandracchia, B. Nottelet, F. Innocente, R. Gurny, M. Möller, B. H. Walpoth, *J. Dev. Biol.* **2016**, *4*, 11.

[43] C. Espíndola, A. J. Correa, M. López-López, P. López-Cornejo, E. Bernal, J. A. Lebrón, F. J. Ostos, M. R. E. I. Benhnia, M. L. Moyá, *Pharmaceutics* **2022**, *14*, 2806.

[44] S. Gopalakrishnan, A. Gupta, J. M. V. Makabenta, J. Park, J. J. Amante, A. N. Chattopadhyay, D. Matuwana, C. J. Kearney, V. M. Rotello, *Adv. Healthcare Mater.* **2022**, *11*, 22010 60.

[45] M. C. P. Brugmans, S. H. M. Söntjens, M. A. J. Cox, A. Nandakumar, A. W. Bosman, T. Mes, H. M. Janssen, C. V. C. Bouten, F. P. T. Baaijens, A. Driessen-Mol, *Acta Biomater.* **2015**, *27*, 21.

[46] T. B. Wissing, V. Bonito, E. E. van Haaften, M. van Doeselaar, M. M. Brugmans, H. M. Janssen, C. V. Bouten, A. I. Smits, *Front. Bioeng. Biotechnol.* **2019**, *7*, https://doi.org/10.3389/fbioe.2019.00087.

[47] J. Marzi, E. C. Munnig Schmidt, E. M. Brauchle, T. B. Wissing, H. Bauer, A. Serrero, S. H. M. Söntjens, A. W. Bosman, M. A. J. Cox, A. I. P. M. Smits, K. Schenke-Layland, *Front Cardiovasc. Med.* **2022**, *9*.

[48] A. M. Fea, J. I. Belda, M. Rekas, A. Jünemann, L. Chang, L. Pablo, L. Voskanyan, L. J. Katz, *Clinic. Ophthalmol.* **2014**, *8*, 875.

[49] C. K. Bahler, C. R. Hann, T. Fjield, D. Haffner, H. Heitzmann, M. P. Fautsch, *Am. J. Ophthalmol.* **2012**, *153*, 1206.